

Quick Retrieval of Effective Electromagnetic Metamaterial Parameters by Using a Multi-fidelity Surrogate Modelling Approach

Giovanni Angiulli¹, Mario Versaci², Salvatore Calcagno², and Paolo Di Barba³

¹ Department of Information Engineering, Infrastructures and Sustainable Energy, Mediterranean University, Italy

² Department of Civil, Energetic, Environmental and Material Engineering, Mediterranean University, Italy

³ Department of Electrical, Computer and Biomedical Engineering, University of Pavia, Italy

Received: date / Revised version: date

Abstract. Electromagnetic metamaterials (MMs) are artificial composites that exhibit exceptional physical characteristics. Their design, which relies on the retrieving of the effective medium parameters, is usually a very time-consuming process because of the high number of full-wave simulations involved in this task. To alleviate the related computational burden, we propose to use a Multi-fidelity Surrogate Modelling (MFSM) approach. Numerical results demonstrate that this methodology turns out to be promising for a quick evaluation of the scattering parameters from which the effective constitutive parameters of a MM are retrieved, as shown by two numerical examples.

PACS. XX.XX.XX No PACS code given

1 Introduction

Because of their uncommon physical characteristics and variety of potential applications, a huge research activity about electromagnetic Metamaterials (MMs) has been carried out by the scientific community during the last decades [1], [2]. In essence, a MM consists of a lattice of elementary inclusions hosted in a dielectric medium [1–4]. Being these objects (and their mutual distances) far smaller than the wavelength of the outer excitation field, a MM is usually modelled as a continuous media characterized by an effective electrical permittivity $\epsilon_{eff}(f)$ and a magnetic permeability $\mu_{eff}(f)$ [1], [2], despite the limitation of this approach [5].

The design process of a MM, which consists of assigning it a well-defined effective medium parameters frequency behaviour, is carried out through the optimization of a suitable cost function [6–10]. By recovering the effective constitutive parameters for a MM through the knowledge of related scattering matrix, its unit cell geometry is shaped until an extremum for the cost function is reached [6–10]. Very recently, to overcome the computational burden usually involved in this process, the Surrogate Model (SM) paradigm has been proposed [10], [11]. A SM is a reasonably accurate and computationally light numerical model that can be used instead of the exact, but computationally expensive, numerical model derived from the physics of the phenomenon under analysis in all those design tasks where a great number of simulations are required [12], [13]. Even if running a physical model at a

high level of precision and exploiting the data it provides, it is a possible strategy to build a SM, often the generation of these data results to be very time-consuming [13]. The Multi-Fidelity Surrogate Modelling approach (MFSM) allows combining the requirement to generate data for training a SM with a reduced computational effort (at this purpose running with different levels of accuracy the physical model) with its modelling precision [13].

In this paper, we investigate the performances of the MFSM approach in the perspective of a quick evaluation of the scattering parameters for a MM in order to speed up the overall computation process related to the computation of its effective constitutive parameters $\mu_{eff}(f)$ and $\epsilon_{eff}(f)$. The paper is organized as follows: in section 2, we briefly discuss of the SM techniques by using Kernel methods [14]. The choice to use kernels as SMs in this work is mainly due to their ability to model in a more effective way the non-linear input-output relationship occurring in complex devices and systems, compared with other SM techniques, and by the fact that they are less prone to the curse of dimensionality [14]. In section 3, an account of the MFSM approach is given. Numerical results are shown in section 4. Finally, in section 5 some considerations are drawn.

2 Surrogate Modelling and Kernels

In microwave and optical engineering, procedures as statistical analysis, yield-driven design, parametric design,

Table 1. Kernel and assigned parameters used in this study

Name	Kernel	Parameters
Gaussian	$\exp(-\varepsilon^2 \ \mathbf{x} - \mathbf{x}'\ ^2)$	$\varepsilon = 3.0$
Matérn	$\frac{K_{d/2-\beta}^a(\varepsilon \ \mathbf{x} - \mathbf{x}'\)}{(\varepsilon \ \mathbf{x} - \mathbf{x}'\)^{d/2-\beta}}$	$\varepsilon = 4.0, \beta = 2$

^a $K_{d/2-\beta}$ is the modified Bessel function [14].

optimization require a high number of accurate full-wave numerical computations. Although the modern microprocessor technology provides more and more powerful CPUs, the above processes very frequently represent a bottleneck towards the efficient design of high-performance systems and devices [12]. In this frame of reference, the Surrogate Modelling approach is useful to reduce the CPU time involved in these tasks, by replacing the accurate high-fidelity (HF) simulations based on Maxwell equations discretization by projective methods (i.e. Method of Moments, Finite Element Method, Finite Difference Method) [16] with a suitable numerical model, the so-called Surrogate Model (SM), computationally lighter and faster to evaluate [12], [13]. Neural networks, fuzzy neural networks, linear regression models, and Kriging methods [17–21] are examples of SMs usually employed to this aim.

Kernels methods, exploited in a number of fields ranging from approximation theory to machine learning [14], provide a more general framework in which the Surrogate Modelling approach can be set, looking at it like a scattered data fitting problem, i.e. given the set $\{\mathbf{x}_i, y_i\}_{i=1}^N$ where the elements $\mathbf{x}_i \in \mathbb{R}^d$ are called *data sites* and the elements $y_i \in \mathbb{R}$ are called *data values* (which represent the set of the input-output pairs related to the physical model computer simulations runs required to analyze a given system or device), the objective is to find a functional relationship $\mathcal{P}(\cdot)$ such that $\mathcal{P}(\mathbf{x}_i) = y_i, i = 1, \dots, N$. Taking into account of the result of the Haar-Mairhubert-Curtis theorem [14], $\mathcal{P}(\cdot)$ can be written as a linear combination of suitable basis functions, $\mathcal{K}(\cdot, \mathbf{x}_1), \dots, \mathcal{K}(\cdot, \mathbf{x}_N)$, which depend from the data sites, named *kernel functions*, as

$$\mathcal{P}(\mathbf{x}) = \sum_{p=1}^N \alpha_p \mathcal{K}(\mathbf{x}, \mathbf{x}_p) \quad \mathbf{x} \in \mathbb{R}^d \quad (1)$$

Evaluating the expansion coefficients as $\boldsymbol{\alpha} = \mathbf{K}^{-1}\mathbf{y}$, with $(\mathbf{K})_{i,p} = \mathcal{K}(\mathbf{x}_p, \mathbf{x}_i)$ and $\mathbf{y} = (y_1 \dots, y_N)^t$, we can write the kernel interpolant (1) as

$$\mathcal{P}(\mathbf{x}) = \boldsymbol{\xi}^t(\mathbf{x})\mathbf{K}^{-1}\mathbf{y} \quad (2)$$

with $\boldsymbol{\xi}(\mathbf{x})^t = (\mathcal{K}(\mathbf{x}, \mathbf{x}_1), \dots, \mathcal{K}(\mathbf{x}, \mathbf{x}_N))$, obtaining, in this way, a model for the HF data input-output relationship. For a deeper discussion of kernel methods and surrogate modelling the reader can refer to [14] and references within.

3 The Multi-fidelity Surrogate Modelling approach

To provide a response comparable with that of the physical model we want to emulate, a SM often need of a large amount of HF data, often heavy to obtain in term of CPU time. The Multi-Fidelity Surrogate Modelling (MFSM) approach allows to alleviate this problem by combining between them a large amount of low fidelity (LF) data, computed in a fast way running the physical model with a low level of resolution, with few HF samples, this time evaluated by using a high level of resolution, in a reasonable CPU time [13].

Two are the possible approaches for realizing an MFSM: the deterministic and the probabilistic one. Following [13], the MFSM based deterministic approach can be concisely described through a two-step procedure. In the first step, two sets of data are collected: the set of LF data $\mathbf{TS}_{LF} = \{\mathbf{x}_i, y_i^{LF}\}_{i=1}^N$ and the set of HF data $\mathbf{TS}_{HF} = \{\mathbf{x}_i, y_i^{HF}\}_{i=1}^M$ (with $M \ll N$), which are obtained by executing the computational model based on the physical model in a low-fidelity (LF) and a high-fidelity (HF) modality (the different levels of fidelity can be usually obtained acting on the level of discretization of the computational domain). At this stage, a SM, denoted in the following as \mathbf{SM}_{LF} , can be built using the \mathbf{TS}_{LF} data, if necessary [10]. In the second step, a suitable SM able to correct the response provided by the LF model (or by the \mathbf{SM}_{LF} previously developed), is developed. This can be done by using the dataset built on the difference among y_i^{LF} and y_i^{HF} corresponding to the points $\mathbf{x}^{(i)} \in \mathbf{TS}_{LF} \cap \mathbf{TS}_{HF}$. In other words, we have that

$$\mathbf{HF}(\mathbf{x}) = \mathbf{SM}_{LF}(\mathbf{x}) + \delta(\mathbf{x}) \quad (3)$$

thus realizing the so-called additive correction multi-fidelity model. The SM $\delta(\mathbf{x})$ is called additive function or discrepancy function. Alternatively, the ratio between y_i^{HF} and y_i^{LF} corresponding to the points $\mathbf{x}^{(i)} \in \mathbf{TS}_{LF} \cap \mathbf{TS}_{HF}$, can be exploited. Accordingly, we have that

$$\mathbf{HF}(\mathbf{x}) = \rho(\mathbf{x})\mathbf{SM}_{LF}(\mathbf{x}) \quad (4)$$

thus realizing the so-called multiplicative correction multi-fidelity model. The SM $\rho(\mathbf{x})$ is called multiplicative function. A comprehensive correction approach

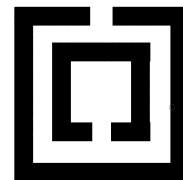


Fig. 1. Unit cell layout for the μ -negative MM composed by square ring resonators from [23]: outer ring length = 3 mm; rings widths = 0.25 mm; gap size = 0.5 mm; distance between rings = 0.5 mm. Substrate characteristics: $\epsilon_r = 3.84$, thickness = 0.25 mm.

$$\text{HF}(\mathbf{x}) = \rho(\mathbf{x})\text{SM}_{LF}(\mathbf{x}) + \delta(\mathbf{x}) \quad (5)$$

where both $\rho(\mathbf{x})$, and $\delta(\mathbf{x})$, are employed, is also possible.

Probabilistic approach includes Bayesian and Co-Kriging techniques [9]. The reader interested to these last methods can refer to [12], [22] and references within.

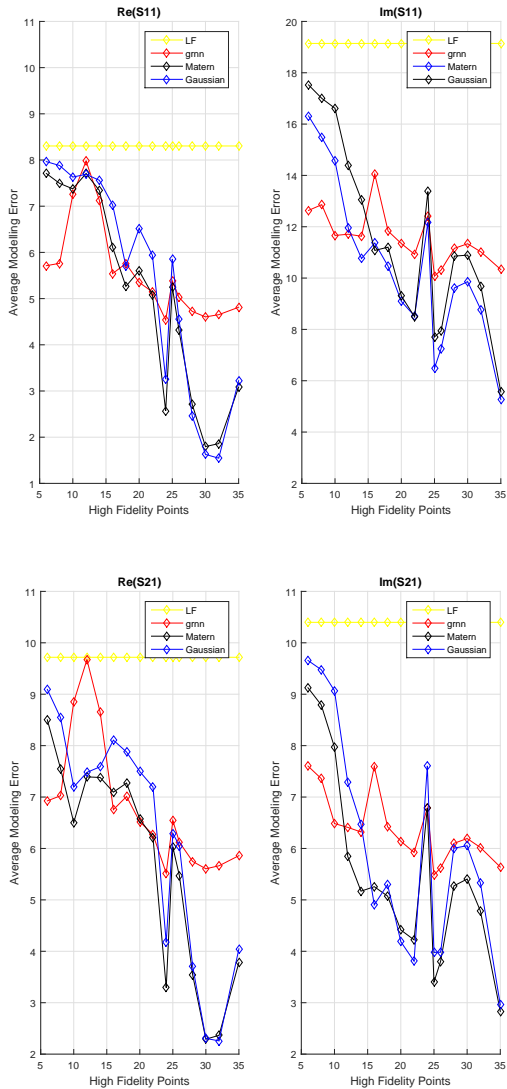


Fig. 2. Average modelling error versus the number of high fidelity data points exploited to build the discrepancy function $\delta(f)$ for the MFSM calculations of the scattering parameters of the μ -negative MM of Fig.(1): red curve: GRNN; black curve: Matérn kernel; blue curve: Gaussian kernel (yellow curve: Low fidelity average modelling error).

Table 2. Scattering parameters average modelling error using $n_p = 35$ HF samples for the μ negative MM of Fig.1.

Real Part - S11				
	LF			
	LF	8.304%		
MF	GRNN	Matérn	Gaussian	
Add.	4.813%	3.084%	3.223%	
Mul.	13.182%	13.623%	16.055%	
Dir.	10.711%	4.545%	12.085%	
Imaginary Part - S11				
	LF			
	LF	19.143%		
MF	GRNN	Matérn	Gaussian	
Add.	10.332%	5.268%	5.563%	
Mul.	14.974%	11.163%	15.197%	
Dir.	24.384%	10.849%	16.729%	
Real Part - S21				
	LF			
	LF	9.718%		
MF	GRNN	Matérn	Gaussian	
Add.	5.860%	3.783%	4.049%	
Mul.	7.038%	5.998%	12.094%	
Dir.	16.73%	4.302%	11.583%	
Imaginary Part - S21				
	LF			
	LF	10.398%		
MF	GRNN	Matérn	Gaussian	
Add.	5.639%	2.831%	2.957%	
Mul.	9.925%	8.185%	11.695%	
Dir.	13.287%	6.923%	13.41%	

4 Results

In this section, numerical results relevant to the performances provided by an MFSM approach based on the additive correction compared with those provided by the multiplicative correction, and by a standard SM made up exploiting a suitable set of high fidelity data (HF-SM), are given. The Matérn and the Gaussian kernels [14] have been selected to implement the discrepancy function $\delta(f)$, the multiplicative function $\rho(f)$, and the HF-SMs exploited in our study. Their functional expression and the values of the related parameters are reported in Table 1¹. Furthermore, a more classical approach based on neural network theory, by using a generalized regression neural network (GRNN) (which is commonly employed in approximation theory) [24], has been exploited, and its performances compared with those of the kernels above mentioned. The Kramers-Kronig retrieving algorithm described in [15] has been used to recover the effective constitutive parameters $\epsilon_{eff}(f)$, $\mu_{eff}(f)$ from the knowledge of the scattering parameters for all the MMs structures considered in this work. All the numerical simulations have been carried out by using the MATLAB environment and the toolbox package developed in [16]. The average modelling error measure

$$\frac{\|\bar{\mathbf{R}}(f) - \hat{\mathbf{R}}(f)\|}{\|\bar{\mathbf{R}}(f)\|} \%, \quad (6)$$

¹ ε is the shape parameter, β controls the kernel smoothness and d is the space dimension [14] ($d=1$ in this case) [14].

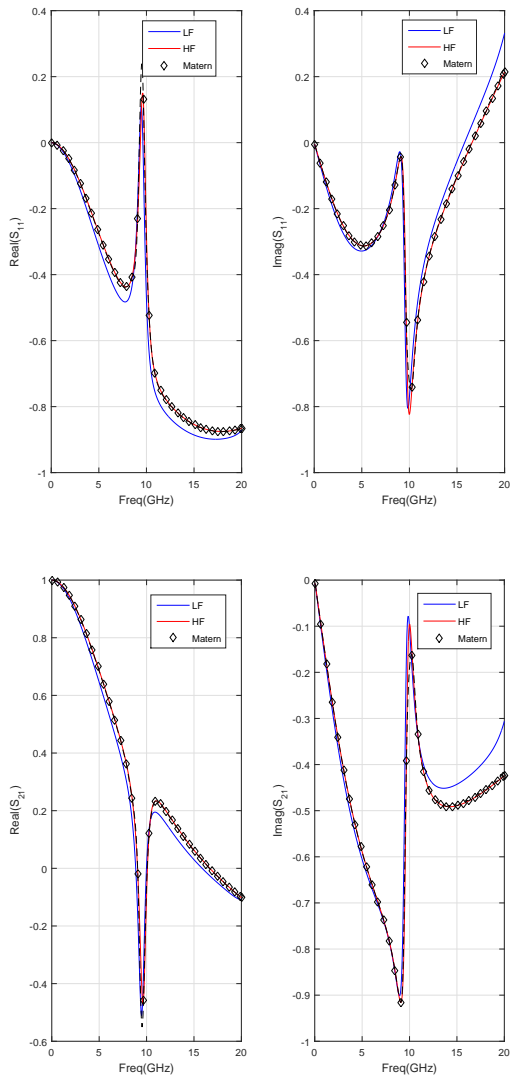


Fig. 3. Real and imaginary parts of the scattering parameters over the frequency range from 0 Hz to 20 GHz for the μ -negative MM of Fig.(1): top left side: $\text{Re}(S_{11})$, top right side: $\text{Im}(S_{11})$. Bottom left side: $\text{Re}(S_{21})$, bottom right side: $\text{Im}(S_{21})$. Red line: High fidelity result, Blue line: low fidelity result, black diamond: additive correction based MFSM result.

with $\bar{\mathbf{R}}(f)$ and $\hat{\mathbf{R}}(f)$ denoting the HF and the MFSM (or the SM) response, respectively, has been used as criterion to assess the quality of the different approaches considered in this work [22].

As a first case, we have considered a μ -negative MM composed by the periodic arrangement of square split ring resonators [23] (Fig. (1) reports the unit cell geometrical dimensions and the substrate dielectric characteristics). The structure has been simulated using the software ANSYS HFSS, running on an Intel Xeon DP E5405 Quad Core 2.0 based workstation, with 20 GB of main memory. The scattering parameters S_{11} , S_{21} have been computed in the frequency range from 0 Hz to 20 GHz. Following what has

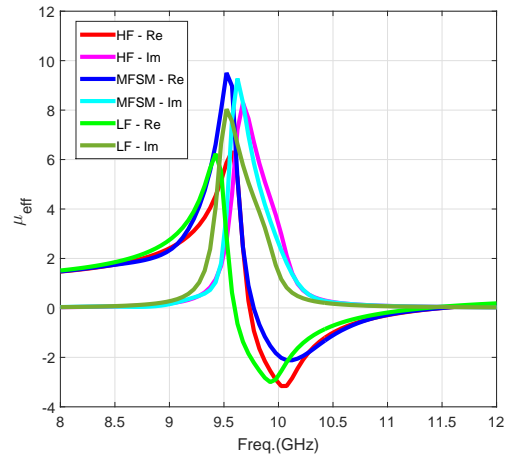


Fig. 4. Retrieved effective $\mu_{eff}(f)$ for the μ -negative MM of Fig.(1)

been stated in section 3, the different levels of fidelity has been obtained using different mesh sizes: 2505 tetrahedra for the LF case, and 32051 tetrahedra for the HF case, respectively. Fig. (2) shows the behaviour of the scattering parameters average modelling error as a function of the number n_p of high fidelity data points (evenly sampled over the considered frequency range) exploited to build the discrepancy function $\delta(f)$ employed in (3). Although the average error decreases as the number of high fidelity points increases, it can be noticed that this trend results to be quite erratic for all the modality of implementation for the discrepancy function $\delta(f)$ (the exploited kernels' parameters are reported in Table 1, whereas the spread factor for the GRNN was 0.9 [24]). Setting a threshold not exceeding the 6% as a tolerable value for the overall average modelling error (this value represents a trade-off between the obtained accuracy and the time needed to evaluate the HP samples required to train $\delta(f)$), the best result for both for the real and the imaginary part of the scattering parameters has been provided by the Matern kernel, in correspondence of a number of HF samples $n_p = 35$. Table 2 shows the comparison among the scattering parameters average modelling errors provided by both the additive and the multiplicative MFSMs and by the HF-SMs developed in this study (these values are reported in the rows labelled with "Add", "Mul", and "Dir.", respectively, of table 2). The superiority of the additive MFSM approach by using the Matern kernel is apparent. Fig. (3) show a graphical comparison among the real and imaginary parts of the scattering parameters computed by both the LF and HF surrogate models, and by the additive MFSM model (all based on the Matern kernel) exploiting $N_p = 400$ points over the frequency range from 0 Hz to 20 GHz. It can be noticed as the MFSM results are in very good agreement with the HF ones but obtained with a computational time $t_{MFSM} = 4$ min. and 22 sec. (which is given by the sum between the computational time involved by the LF computation, $t_{LF} = 32$ sec., and

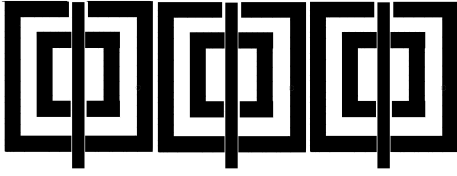


Fig. 5. Three unit cells layout for the double negative MM slab from [15]: outer ring resonator length = 2.2 mm; rings widths = 0.2 mm; gap size = 0.3 mm; distance between rings = 0.15 mm. Wire width = 0.14 mm. Substrate characteristics: $\epsilon_r = 4.4$, thickness = 0.75 mm.

the time required to set up the discrepancy function $\delta(f)$, $t_\delta = 3.50$ min.) that is more than halved if compared with the time $t_{HF} = 11$ min. required by the HF computation (the speed-up factor is equal to $\frac{t_{HF}}{t_{MFSM}} \approx 2.58$). Fig. (4) shows a graphical comparison between the real and the imaginary part of the retrieved $\mu_{eff}(f)$, in a frequency band around the first resonance, by using the LF, the HF and the MFSM computed scattering parameters, respectively. As it can be observed, the MFSM result is better closer to the HF equivalent permittivity than the LF one.

As the second case of study, we have considered a double-negative MM realized by the periodical arrangement of three split-ring resonators and three metallic wires reciprocally interleaved [15] (the geometrical dimensions and the substrate dielectric characteristics are reported in Fig. (5)). Considering that this MM structure was three times thicker than the previous one [15], the different levels of fidelity have been realized by using, in this case, a num-

Table 3. Scattering parameters average modelling error using $n_p = 81$ HF samples for the double negative MM of Fig.5.

Real Part - S11				
	LF	18.527%		
MF	GRNN	Matérn	Gaussian	
Add.	14.655%	1.312%	1.506%	
Mul.	19.788%	13.407%	15.359%	
Dir.	18.065%	2.319%	2.279%	
Imaginary Part - S11				
	LF	27.517%		
MF	GRNN	Matérn	Gaussian	
Add.	22.075%	5.547%	4.807%	
Mul.	119.131%	109.945%	134.256%	
Dir.	27.094%	2.437%	2.846%	
Real Part - S21				
	LF	25.7756%		
MF	GRNN	Matérn	Gaussian	
Add.	20.814%	1.384%	2.293%	
Mul.	51.876%	26.042%	29.068%	
Dir.	24.612%	2.045%	2.367%	
Imaginary Part - S21				
	LF	24.985%		
MF	GRNN	Matérn	Gaussian	
Add.	20.617%	5.112%	4.456%	
Mul.	201.486%	123.533%	168.325%	
Dir.	23.863%	3.081%	2.951%	

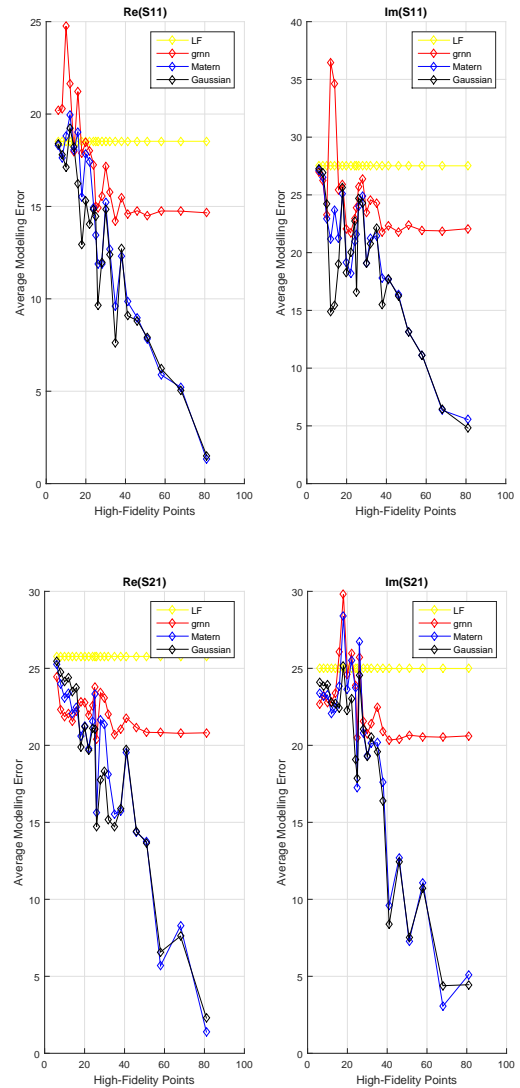


Fig. 6. Average modelling error versus the number of high fidelity data points exploited to build the discrepancy function $\delta(f)$ for the MFSM calculations of the scattering parameters of the double negative MM of Fig. (5): red curve: GRNN; black curve: Matérn kernel; blue curve: Gaussian kernel (yellow curve: Low fidelity average modelling error).

ber of tetrahedra far larger than in previous case (58548 tetrahedra for the LF simulations and 198727 tetrahedra for the HF simulations, respectively). Fig.(6) reports the behaviour of the scattering parameters average modelling error. We can note that it has a more regular trend compared with that of Fig.(2). In correspondence of the value $n_p = 81$, the Gaussian kernel provides the best trade-off result in term of overall average modelling error (also for this MM structure the error has been subjected to the constraint not to exceed the 6% threshold), although, on the basis of the results shown in Table 3, the performances of the MFSM are comparable with those provided by the HF-SM built exploiting the same Gaussian kernel. Fig.(7)

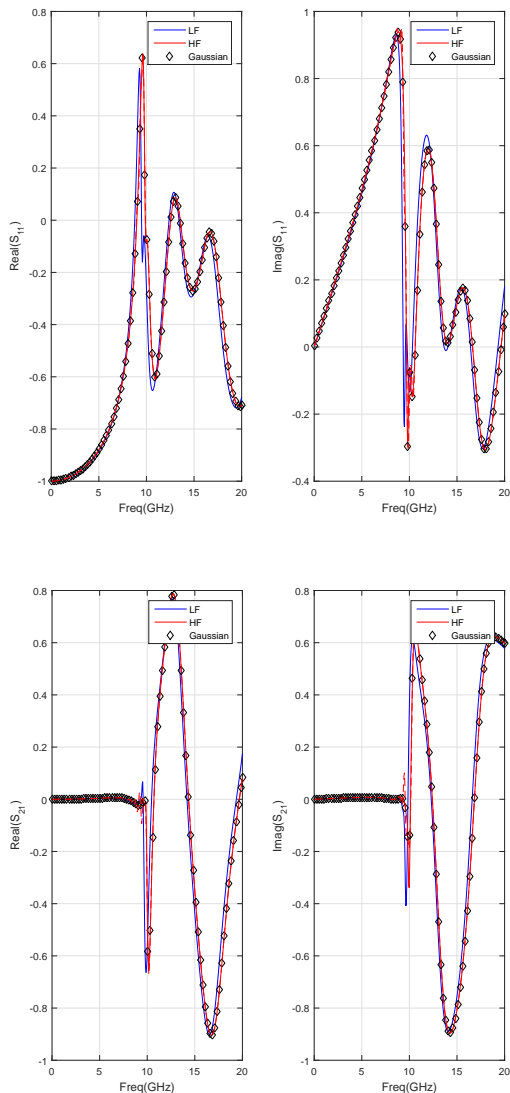


Fig. 7. Real and imaginary parts of the scattering parameters over the frequency range from 0 Hz to 20 GHz for the double negative MM of Fig.(5): top left side: $\text{Re}(S_{11})$, top right side: $\text{Im}(S_{11})$, bottom left side: $\text{Re}(S_{21})$, bottom right side: $\text{Im}(S_{21})$. Red line: High fidelity result, Blue line: low fidelity result, black diamond: additive correction based MFSM result.

shows a graphical comparison among the real and imaginary parts of the scattering parameters provided by both the LF and HF surrogate models, and by the additive MFSM model (all based on the Gaussian kernel) exploiting $N_p = 400$ points over the frequency range from 0 Hz to 20 GHz. Also, here, the MFSM provides results that are in very good agreement with the HF ones but obtained quicker. Precisely, the MFSM computational time t_{MFSM} was of 2 hours and 5 minutes (this time resulted by the sum between the computational time related to the LF computation, $t_{LF} = 31$ min., and by the time required to set up the discrepancy function $\delta(f)$, $t_\delta = 1.44$ hours),

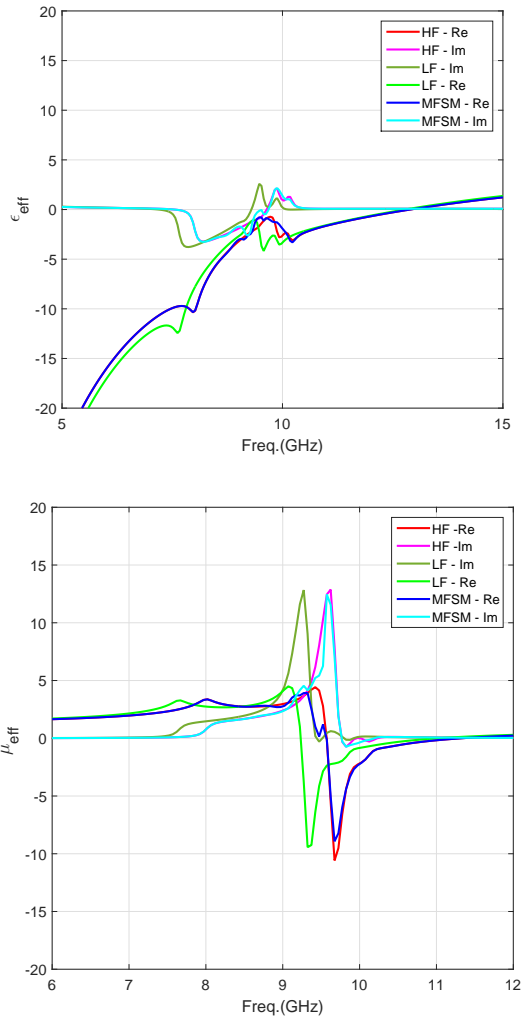


Fig. 8. Retrieved effective parameters for the double negative MM of Fig.(5). Top: $\epsilon_{eff}(f)$. Bottom: $\mu_{eff}(f)$.

whereas the computational time t_{HF} was of 5 hours and 38 minutes, with a speed-up factor equal to $\frac{t_{HF}}{t_{MFSM}} \approx 2.46$). Finally, fig.(8) shows a comparison among the real and the imaginary part of $\epsilon_{eff}(f)$ and $\mu_{eff}(f)$ retrieved by using the LF, HF and the MFSM computed scattering parameters, in a frequency interval around the first resonance. Also, for this last case, the MFSM and HF results are very close to each other.

5 Conclusions

In this work, an MFSM approach has been considered in order to retrieve the effective electromagnetic parameters of a MM slab quickly. This methodology has been validated, considering two examples of MM structures.

Two kinds of kernels have been exploited to this purpose, the Matérn, and the Gaussian, respectively. Their performances have been compared with those provided by

a standard way to realize a SM. At this purpose, a GRNN has been employed. The results obtained in term of computational saving by using the additive MFSSM approach is quite promising, although controversial in the case of thick MM slab. Because of their simplicity, in this study, only the additive and multiplicative MFSSMs methods have been exploited. A comparison with other Multi-fidelity approaches (i.e., Co-Kringing) and an analysis of the influence of the parameters ε and β will be considered in a future work.

6 Authors contributions

All the authors were involved in the preparation of the manuscript. All the authors have read and approved the final manuscript.

References

1. F. Capolino, *Theory and Phenomena of Metamaterials* (CRC Press, 2009)
2. S. Anantha Ramakrishna, T. M. Grzegorzczak, *Physics and Applications of Negative Refractive Index Materials* (CRC Press, 2008)
3. A. Sgró, D. De Carlo, G. Angiulli, F. C. Morabito, M. Versaci, *Multidisciplinary Approaches to Neural Computing*, **69**, 47 (2017)
4. M. Rizwan, Yan-Kun Dou, Hai-Bo Jin, Zhi-Ling Hou, Ling-Bao Kong, Jing-Bo Li, F. K. Butt, and F. Rehman *The European Physical Journal Applied Physics*, **63**, 10502, (2013).
5. C. R. Simovski, C. R., *Optics and Spectroscopy*, **107**, 726 (2009)
6. W. Wang, W. K. Xu, and H. Hai, *The European Physical Journal-Applied Physics*, **53**, 20401, (2011).
7. P. Y. Chen, C. H. Chen, H. Wang, H., J. H. Tsai J.H., Ni. Wei-Xin, *Optics express*, **16**, 12806 (2008)
8. S. Zhou, W. Li, Y. Chen, G. Sun, Q. Li, *Acta Materialia*, **59**, 2624 (2011)
9. S. D. Campbell, D. Sell, R. P. Jenkins, E. B. Whiting, J. A. Fan, D. H. Werner, *Optical Materials Express*, **9**, 1842 (2019)
10. K. Diest, *Numerical Methods for Metamaterial Design* (Springer, 2013)
11. G. Angiulli, M. Versaci, S. Calcagno, P. Di Barba, *Metamaterial unit cell characterization by using a multi-fidelity surrogate modelling approach*, in *Proceedings 19th Symposium on Electromagnetic Fields in Mechatronics, Electrical and Electronic Engineering*, 2019
12. S. Koziel, and X. S. Yang, *Computational optimization, methods and algorithms* (Springer, 2011)
13. M. G. Fernandez-Godino, C. Park, N. H. Kim, R. T. Haftka, "Review of multi-fidelity models," arXiv preprint arXiv:1609.07196, 2016.
14. G. E. Fasshauer, and M. McCourt, *Kernel-Based Approximation Methods Using MATLAB* (World Scientific Publishing, 2015)
15. Z. Szabó, G. H. Park, R. Hedge, R., E. P. Li, *IEEE Transactions on Microwave Theory and Techniques*, **58**, 2646 (2010)
16. X. Q. Sheng, W. Song, *Essentials of computational electromagnetics*, John Wiley & Sons, 2011.
17. G. Amendola, G. Angiulli, E. Arnieri, L. Boccia, D. De Carlo, *Prog. Electromagn. Res. C*, **42**, 1 (2013)
18. G. Angiulli, M. Versaci, *International Journal of Infrared and Millimeter Waves*, **23**, 1513 (2002)
19. G. Amendola, G. Angiulli, E. Arnieri, L. Boccia, L., D. De Carlo, *Prog. Electromagn. Res. C*, **43**, 165 (2013)
20. G. Domènech-Asensi, J. Hinojosa, J. Martinez-Alajarn, J. Garrigós-Guerrero, *IEEE Transactions on Microwave Theory and Techniques*, **53**, 3305 (2005).
21. G. Angiulli, D. De Carlo, D., A. Sgró, M. Versaci, F. C. Morabito, *IEICE Electronics Express*, **14**, 20170073 (2017)
22. I. Couckuyt, S. Koziel, T. Dhaene, *International Journal of Numerical Modelling: Electronic Networks, Devices and Fields*, **26**, 64 (2013)
23. Z. Szabó, J. Fuzi, *IEEE Transactions on Magnetics*, **50**, 1 (2014)
24. W. Zhang, *Computational ecology: artificial neural networks and their applications*, World Scientific, 2010.